

Terahertz metasurface enabled by barium strontium titanate ferroelectric film

Yuan Fu¹, Xiaojian Fu^{1,*} , and Yunsheng Guo^{2,**}

¹ State Key Laboratory of Millimeter Waves, Southeast University, Nanjing 211189, PR China

² School of Electronic Information Engineering, Inner Mongolia University, Hohhot 010021, PR China

Received: 28 October 2025 / Accepted: 21 January 2026

Abstract. In this paper, a $\text{Ba}_{0.5}\text{Sr}_{0.5}\text{TiO}_3$ (BST) ferroelectric film is prepared and characterized in the terahertz band. Subsequently, based on the prepared BST film, a metasurface is proposed to manipulate electromagnetic waves. The experimental results indicate that the designed BST metasurface can effectively achieve abnormal beam reflection at around 0.750 THz. Furthermore, by taking advantage of the property that the dielectric constant of the BST film can be altered with an external electric field, a programmable metasurface is proposed. By adjusting the dielectric constant of the BST film, the proposed programmable metasurface can achieve a 1-bit phase response within the frequency range of 0.404–0.410 THz. The far-field simulation results demonstrate that the proposed BST programmable metasurface is capable of realizing dynamic beam steering.

Keywords: Terahertz / metasurface / ferroelectric film / beam manipulation

1 Introduction

Metamaterials and metasurfaces have been receiving extensive attention in recent decades due to their unprecedented ability in manipulating electromagnetic waves. By meticulously designing and arranging the patterns, metasurfaces can control the amplitude, phase, polarization, and orbital angular momentum (OAM) of electromagnetic waves, achieving functions such as radar cross section (RCS) reduction [1], abnormal beam deflection [2], non-reciprocal transmission [3–5], energy focusing [6], holographic imaging [7], polarization conversation [8], and vortex beam generation [9,10]. Furthermore, by introducing tunable semiconductor devices like positive-intrinsic-negative (PIN) diodes [11], varactors [12], and field effect tubes (FET) [13], mechanical components such as rotating motors and actuators [14,15], the reconfigurable and programmable metasurfaces have been realized. For example, by switching the state of PIN diode, a programmable metasurface with 2-bit phase resolution has been reported, which can achieve a beam scanning coverage up to $\pm 50^\circ$ at 26.1 GHz [16]. By loading different voltages to alter the capacitance of varactor, a 2-bit programmable metasurface has been proposed to enable dynamic beam steering [17]. Additionally, a micromotor

based multifunctional programmable metasurface has been developed, realizing beam scanning, OAM beam generation, and RCS reduction [18].

As the operating frequency increases into the terahertz frequency band, semiconductor lumped components and mechanical components commonly used in microwave and millimeter wave programmable metasurfaces become ineffective due to significant parasitic effect and limited physical size. As an alternative, some tunable materials like liquid crystal (LC) [19–22], graphene [23,24], phase-change materials such as vanadium dioxide (VO_2) [25–27], germanium telluride (GeTe) [28], as well as micro-electromechanical systems (MEMS) [29] have been applied to enable programmable and reconfigurable metasurfaces. For instance, utilizing the dielectric constant tunability of LC molecules, a terahertz programmable metasurface has been proposed, which can achieve dynamic beam scanning with a coverage range of 20° to 60° at 0.645 THz [21]. By adjusting the Fermi level of graphene, a transmissive programmable metasurface operated at 0.70 THz has been developed to realize dynamic beam scanning and focusing [24]. A VO_2 based programmable metasurface worked at 0.425 THz has been reported, facilitating the deflection of beam over an angle range of 42.8° by varying the temperature distribution [25].

Recently, ferroelectric materials based programmable and reconfigurable devices have garnered significant research interest, owing to their multifold tunability, large tuning range, low power consumption, and fast

* e-mail: fuxj@seu.edu.cn

** e-mail: guoyunsheng@imu.edu.cn

Table 1. The relative parameters of BST film fabrication.

Sputtering pressures	Substrate temperature	RF power	Sputtering time	Annealing temperature	Annealing time
5 mTorr	400 °C	100 W	6 h	650 °C	0.5 h

switching speed [30–36]. For example, utilizing the characteristic that the dielectric constant of ferroelectric film changes with the external electric field, a tunable frequency selective surface based on $\text{Ba}_{0.6}\text{Sr}_{0.4}\text{TiO}_3$ film has been proposed at 12 GHz, capable of beam steering in transmission mode [37]. A $\text{Ba}_{0.5}\text{Sr}_{0.5}\text{TiO}_3$ (BST) film based reconfigurable reflectarray has been developed, which can achieve continuous beam steering from 0° to 25° at 32 GHz [38]. Furthermore, leveraging the property that the dielectric constant of ferroelectric film can be changed with temperature, a $\text{Ba}_{0.6}\text{Sr}_{0.4}\text{TiO}_3$ film enabled thermally tunable spatial filter has been proposed, realizing tuning from 0.826 to 0.905 THz [34].

In this paper, BST ferroelectric film is applied to design terahertz metasurface. At first, a 420-nm-thick BST film is prepared using radio frequency magnetron sputtering technology. The dielectric constant of the fabricated BST film is measured using a terahertz time-domain measurement system. Based on the prepared film, a BST based metasurface is designed, fabricated, and measured. The experimental results indicate that the designed BST metasurface can effectively achieve abnormal reflection of electromagnetic waves at around 0.750 THz. Furthermore, leveraging the tunability of BST film dielectric constant, a terahertz programmable metasurface is proposed, which can achieve a 1-bit phase response at about 0.410 THz. The far-field simulation results demonstrate that the dynamic steering of terahertz waves can be achieved by applying different coding sequences. The relevant results in this study provide a strong impetus for the development of terahertz programmable metasurfaces based on ferroelectric film, showcasing broad application prospects in terahertz wavefront manipulation technology.

2 Material and methods

Radio frequency (RF) magnetron sputtering is applied to prepare the BST film. A 1-inch-diameter sapphire (Al_2O_3) is used as the substrate for depositing the film, which is beneficial to reduce lattice mismatch and thereby facilitating the growth of a high-quality BST film. The main parameters of preparation are summarized in Table 1. The Al_2O_3 substrate is firstly cleaned using chemical reagents to remove impurities. Then, the substrate is put into the deposition chamber and heated to about 400 °C. After 15 minutes of pre-sputtering, the substrate shutter is opened and started to deposit the BST film. The sputtering power is set to 100 W to obtain a moderate deposition rate of BST film. After 6 hours (h) of deposition, the BST film is annealed at 650 °C for 0.5 h in a box oven with an oxygen flow under atmosphere pressure to decrease the defects and improve performance. Finally, a BST film with a thickness of approximately 420 nm is obtained.

3 Results and discussion

3.1 Terahertz dielectric response measurement of BST film

To characterize the dielectric response of the BST film, a terahertz time-domain spectrometer is used. The corresponding measurement setup is shown in Figure 1a. The dielectric constant of the BST film is measured using the transmission method. A picosecond-level time-domain pulse is emitted by the transmitter (Tx), and then received by the receiver (Rx) after passing through the sample. Based on the measured spectra, the dielectric constant of the prepared BST film in the terahertz frequency range can be calculated. The corresponding calculation method can be found in [39]. Figure 1b presents the measured time-domain results in three cases, respectively: air (as a reference), Al_2O_3 , and BST/ Al_2O_3 . It should be noted that due to the weak intensity of terahertz time-domain pulse, the measured dielectric constant values of the prepared BST film exhibit severe fluctuations within the terahertz frequency band. According to reference [40], the dielectric constant of the prepared BST film is set as 400, which is proved to be reasonable in the subsequent design and measurement of the proposed BST metasurface.

3.2 BST metasurface design and measurement

Based on the fabricated BST/ Al_2O_3 sample, a BST metasurface is subsequently designed. Figure 2a presents the designed BST meta-atom, which is consisted of three layers, from top to bottom: BST film, Al_2O_3 , and gold. The corresponding thickness are 420 nm, 226 μm , and 300 nm, respectively. In the simulation, the loss tangent $\tan \delta$ of the prepared BST film is set to 0.02 [37,41]. By changing the side length “ a ” of the top layer BST film, the meta-atom can generate different frequency responses. The simulated amplitude and phase response curves are provided in Figures 2b and 2c, respectively. When $a = 0$, corresponding to no BST film, at this point, the designed meta-atom exhibits resonance around 0.738 THz. On the other hand, when a changes to 200 μm , the resonance frequency of the meta-atom shifts to around 0.698 THz. Correspondingly, the phase response curves appear significant variation in the above two states. Specifically, the designed meta-atom shows amplitude difference of no more than 0.1 and phase difference (corresponding to the ΔPhase curve in Fig. 2c) within $180^\circ \pm 20^\circ$ in the frequency range of 0.706–0.724 THz (corresponding to the gray region), which can be defined as 1-bit phase coding.

To demonstrate the effectiveness of the proposed BST metasurface in manipulating terahertz waves, abnormal beam reflection is simulated. According to the generalized Snell’s law, under the condition of plane wave incident

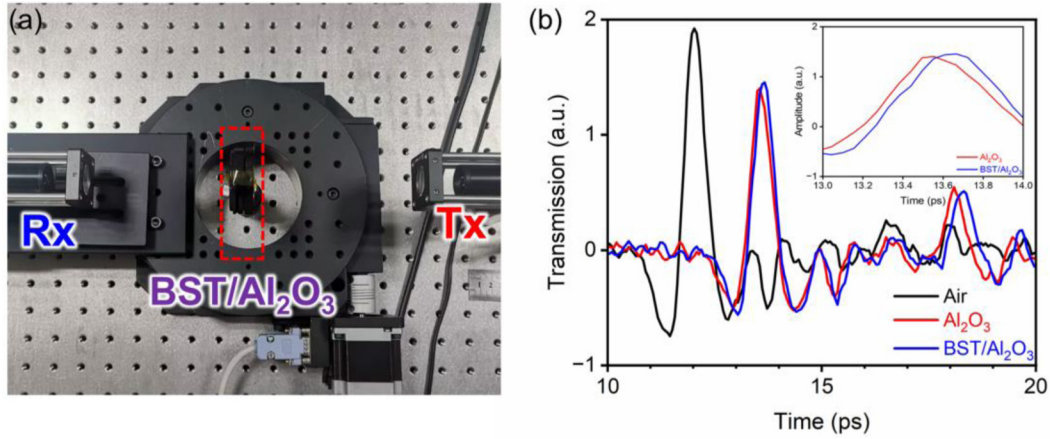


Fig. 1. THz dielectric response measurement of the BST film. (a) The schematic diagram of the measurement setup. (b) The measured THz time-domain transmission spectra.

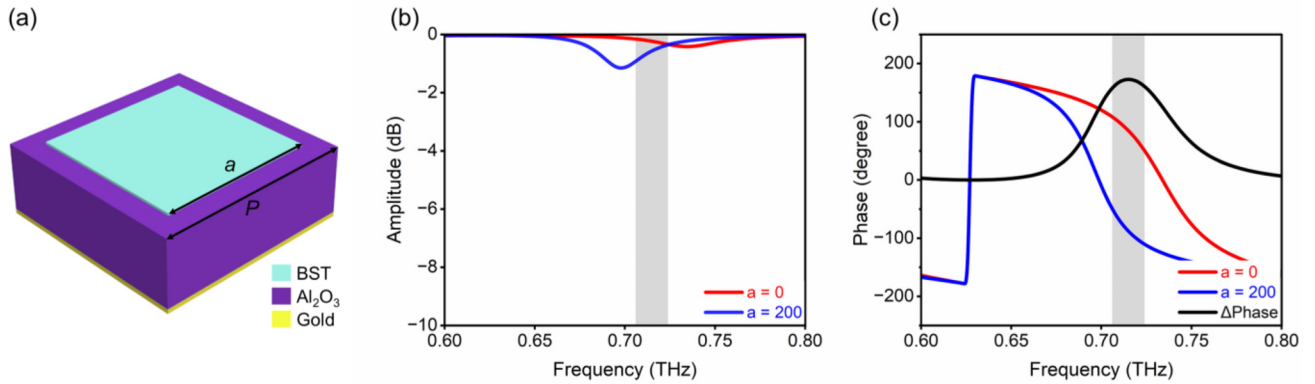


Fig. 2. The proposed BST meta-atom and its simulated amplitude and phase response curves. (a) The structure of the proposed BST meta-atom. The period of the meta-atom is $P = 200 \mu\text{m}$. (b) The simulated amplitude response curves when $a = 0$ and $a = 200 \mu\text{m}$, respectively. (c) The simulated phase response curves and the corresponding phase difference when $a = 0$ and $a = 200 \mu\text{m}$, respectively.

normally, the abnormal reflection angle of a metasurface can be calculated as:

$$\theta = \sin^{-1}\left(\frac{\lambda_0}{\Gamma}\right) \quad (1)$$

where Γ represents the phase gradient period of the metasurface, λ_0 is the working wavelength of the electromagnetic waves in vacuum, and θ is the abnormal reflection angle. In the simulation, an 18×18 array scale is applied, where every two columns of meta-atoms possess the same coding state. As verification, Figure 3a shows the first coding pattern, corresponding to a state of “000000000” coding. At this time, the calculated θ should be 0° , which means the incident waves should be reflected perpendicularly. Figures 3b and 3c respectively present the simulated two-dimensional (2D) and three-dimensional (3D) far-field scattering patterns, where a primary beam can be observed at 0° . Subsequently, a periodic coding of “110011001” is applied, and the corresponding coding pattern is shown in Figure 3d. The phase gradient period Γ is $800 \mu\text{m}$, and the calculated θ should be $\pm 31.4^\circ$ at 0.720 THz . The simulated far-field scattering patterns are demonstrated in Figures 3e and 3f. It can be seen that

the strong perpendicular reflection disappears, replaced by two oblique reflection beams at about $\pm 31.5^\circ$, which is highly consistent with the theoretical calculation.

Subsequently, the fabrication and measurement of the proposed BST metasurface are conducted. The BST film is patterned processing using lithography technique. Figure 4a presents the fabricated BST metasurface along with the corresponding micrograph. To verify the abnormal reflection of the fabricated BST metasurface, the THz time-domain spectroscopy measurement system is applied, as shown in Figure 4b. The Tx illuminates the BST metasurface vertically, while the Rx rotates around the metasurface and simultaneously detects the THz signal reflected to different directions. When the Rx rotates to -30° , a distinct quasi-periodic oscillation waveform is received, as shown in Figure 4c. Next, fast Fourier transform (FFT) is applied to obtain the frequency domain spectrum, which is provided in Figure 4d. It can be observed that, compared with other frequencies, the measured amplitude value is significantly enhanced near 0.750 THz , indicating that the energy of the electromagnetic waves is specifically deflected after manipulation by the BST metasurface. A similar phenomenon can also be observed when the Rx rotates to $+30.5^\circ$, as shown in

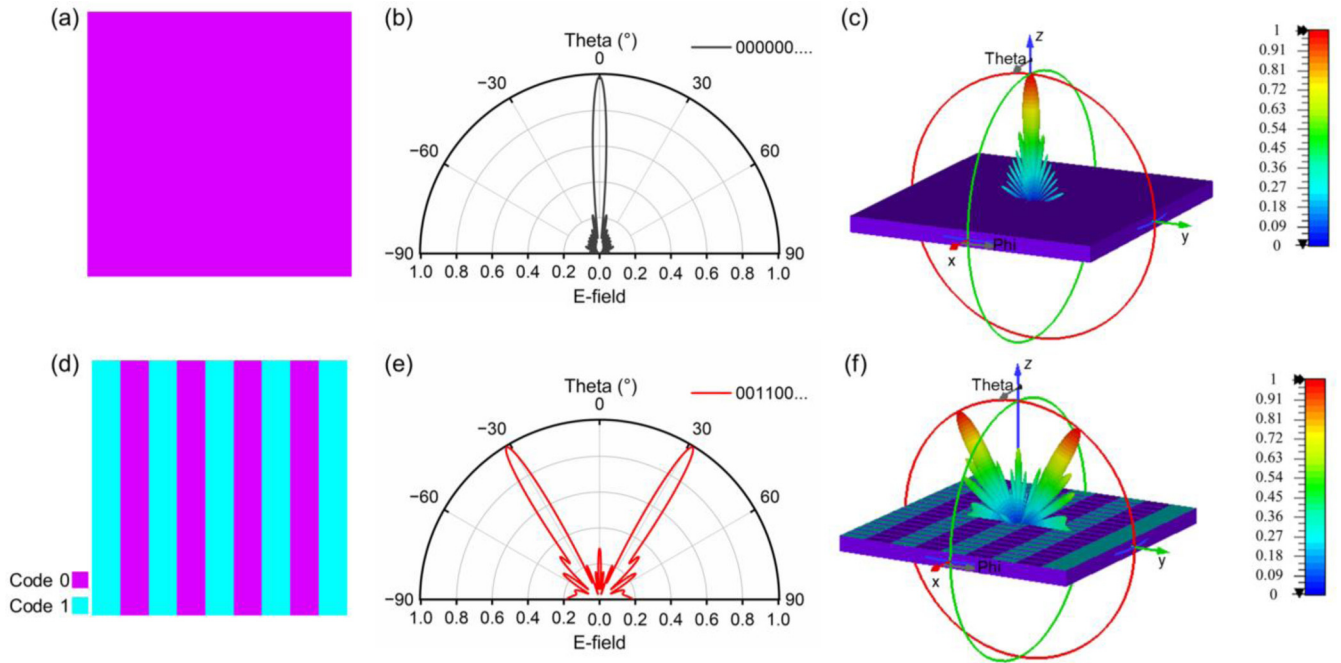


Fig. 3. The abnormal reflection coding patterns and their corresponding far-field scattering patterns. (a) The pattern for “00000000” coding. (b) and (c) The simulated 2D and 3D far-field scattering patterns for “00000000” coding at the operating frequency of 0.720 THz. (d) The pattern for “110011001” coding. (e) and (f) The simulated 2D and 3D far-field scattering patterns for “110011001” coding pattern at the operating frequency of 0.720 THz.

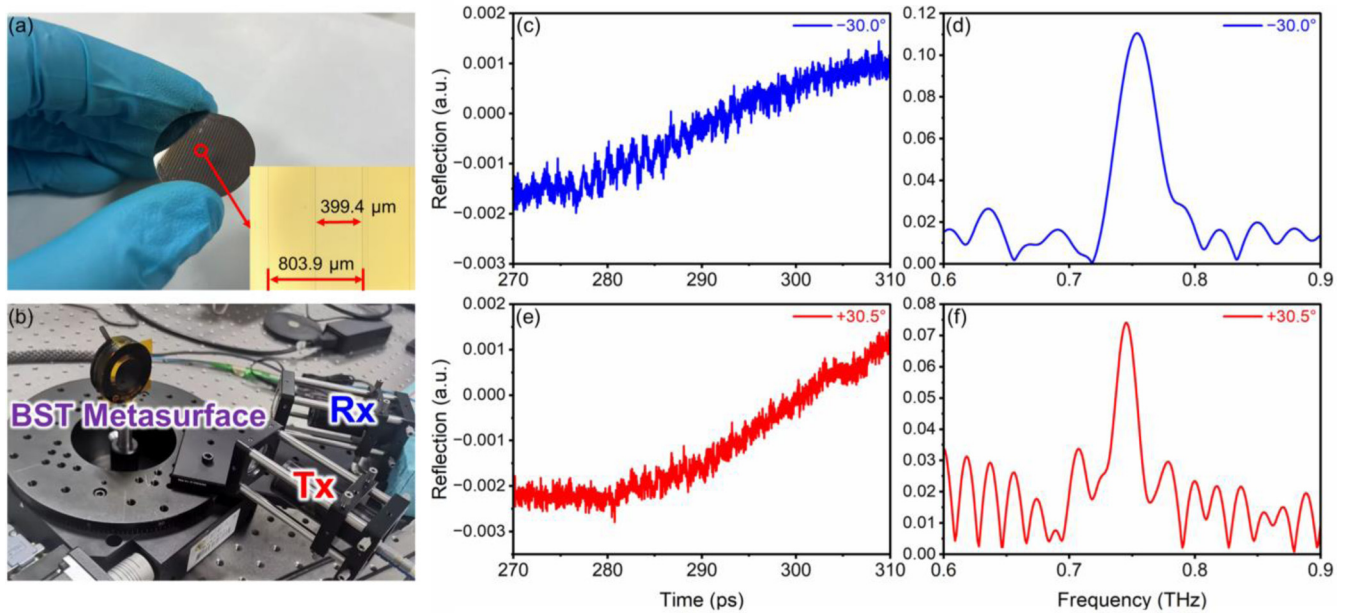


Fig. 4. Characterization and measurement of the BST metasurface. (a) The fabricated BST metasurface and the corresponding optical micrograph. (b) Schematic of the terahertz far-field measurement setup for the BST metasurface. (c) and (d) The measured terahertz reflection time-domain and frequency-domain spectrum at -30.0° . (e) and (f) The measured terahertz reflection time-domain and frequency-domain spectrum at $+30.5^\circ$.

Figures 4e and 4f. It should be noted that compared to the simulated results, a certain frequency shift occurred, which may be caused by the fabrication errors of the BST metasurface and the thickness deviation of Al_2O_3 . Nevertheless, the above results demonstrate the capability of the proposed BST metasurface in manipulating terahertz waves.

3.3 BST programmable metasurface

Furthermore, taking advantage of the property that the dielectric constant of the BST film can be altered by an external electric field, a BST based terahertz programmable metasurface is proposed. Figure 5a illustrates the

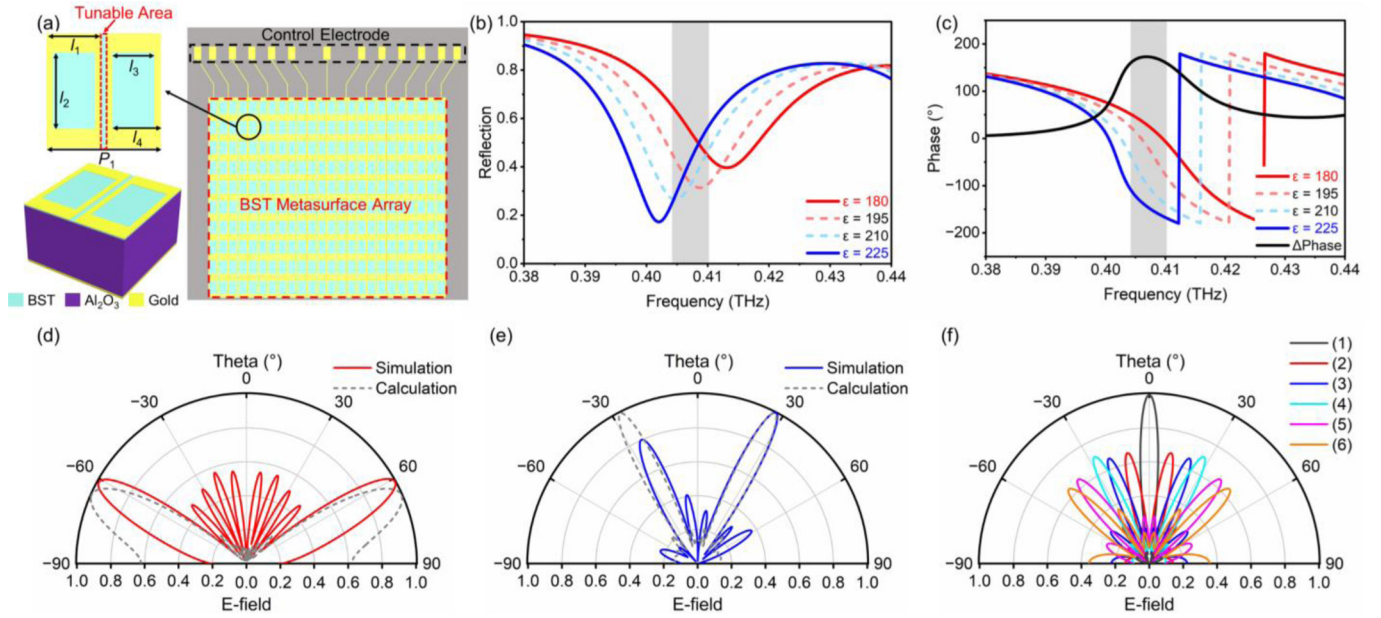


Fig. 5. The design and simulation of the proposed BST programmable metasurface. (a) Structure of the designed meta-atom and bias network, and the specific parameters are $P_1 = 200 \mu\text{m}$, $l_1 = 95 \mu\text{m}$, $l_2 = 128 \mu\text{m}$, $l_3 = 70 \mu\text{m}$, and $l_4 = 85 \mu\text{m}$. (b) and (c) The simulated amplitude and phase response curves of the meta-atom when the dielectric constant “ ϵ ” of the BST film is 180, 195, 210, and 225, respectively. The calculated and simulated far-field scattering patterns of the proposed BST programmable metasurface when the coding sequence is (d) “11001100110” and (e) “11100011100”. (f) The calculated far-field scattering patterns for different coding sequences. The curves (1)-(6) correspond to the calculated reflection angle of 0° , $\pm 10^\circ$, $\pm 20^\circ$, $\pm 30^\circ$, $\pm 40^\circ$, and $\pm 50^\circ$, respectively.

structure of the proposed meta-atom, which is achieved by combining the designed metal pattern with the BST film. The metal pattern is composed of two symmetrical rectangular metal rings on the left and right sides. While achieving specific frequency resonance, they respectively act as the positive and negative electrodes for loading external voltage. In the simulation, the BST film with tunability is set to the rectangular area between two metal rings, as depicted in Figure 5a. Based on the relevant works that previous researchers reported, the dielectric constant tuning range is set varies from 225 to 180, corresponding to a reasonable tuning ratio of 20% [38, 40]. Figures 5b and 5c present the simulated amplitude and phase response curves of the meta-atom, respectively. As the dielectric constant “ ϵ ” changes from 225 to 180, the resonant frequency of the meta-atom shifts from 0.402 to 0.413 THz, resulting in a significant variation in the simulated phase curves accordingly. Particularly, when ϵ is set to 225 and 180, the phase difference of the meta-atom within the frequency range of 0.404-0.410 THz satisfies the condition of 1-bit phase coding.

Subsequently, a BST programmable metasurface consisting of 22×22 meta-atom is simulated, for which every two columns of meta-atoms have the same coding state. Figures 5d and 5e display the simulated far-field scattering patterns when the coding sequence is “11001100110” and “11100011100”, respectively. It can be concluded that different beam pointing can be obtained by switching coding sequences. It is worth noting that for the “11001100110” coding sequence, the calculated θ at 0.410 THz is about $\pm 66.2^\circ$, while the simulated beam pointing in Figure 5d is approximately $\pm 61.0^\circ$. The discrepancy may

Table 2. The calculated coding sequences of different reflection angles.

Reflection angle ($^\circ$)	Required coding sequence
0	0000000000
± 10	00111110000
± 20	01110011100
± 30	11001100110
± 40	11010010010
± 50	10110101001

be caused by both the 1-bit phase quantization errors and the limited array scale. In Figure 5f, the simulated and calculated θ are basically consistent. However, the asymmetric electric field intensity distribution of the simulated beam is observed, which can be ascribed to the intensification of asymmetry of the “11100011100” coding sequence. Overall, by utilizing the tunability of BST dielectric constant, the proposed programmable metasurface can achieve 1-bit phase response, thereby enabling dynamic beam steering in the terahertz band.

Furthermore, the arbitrary beam pointing of the proposed BST programmable metasurface in the one-dimensional (1D) direction can be realized. The reflection angle and the required phase distribution of the metasurface can be calculated as follows:

$$\varphi_m = \frac{2\pi}{\lambda_0} m d \sin \theta \quad (2)$$

where φ_m is the phase of the m th column meta-atom, d represents the period of the meta-atom. For the proposed programmable metasurface, the required coding sequences when θ is 0° , $\pm 10^\circ$, $\pm 20^\circ$, $\pm 30^\circ$, $\pm 40^\circ$, and $\pm 50^\circ$ are calculated and listed in Table 2. As verification, Figure 5f shows the calculated far-field scattering patterns when different coding sequences are applied to the BST programmable metasurface. It can be observed that as the coding sequence changes, the angle of the reflected beam also varies, effectively pointing toward the target direction. It is worth noting that for 1-bit phase coding scheme, symmetrical double-beam reflection is inevitable when a plane wave is incident vertically, which reduces the overall performance of the metasurface. When the phase quantization is increased to 2-bit and higher bit, the metasurface can obtain a better beam manipulation effect, which can be realized jointly by adjusting film preparation process to increase the tuning ratio, and optimizing the structure of the meta-atom to enhance the phase response sensitivity. In terms of hardware implementation, due to the nonlinear response relationship between the dielectric constant of the BST film and the applied electric field, a digital-to-analog converter with high resolution is required to output more precise voltage values.

4 Conclusion

In conclusion, we prepare BST ferroelectric film, and characterize the dielectric response in the terahertz band. According to the measured terahertz transmission spectrum, the dielectric constant of the BST film is determined. Based on the measurement results, a BST metasurface with 1-bit phase response is designed and fabricated. The experimental results show that the designed BST metasurface can effectively achieve abnormal beam deflection around 0.750 THz. Furthermore, by taking advantage of the property that the dielectric constant of BST film can be varied with external electric field, a BST programmable metasurface is proposed. By altering the dielectric constant of the BST film, the proposed metasurface can achieve a 1-bit phase response in the frequency range of 0.404-0.410 THz. The far-field simulation results manifest that the proposed BST programmable metasurface can effectively achieve dynamic scanning of terahertz waves. The above results demonstrate the feasibility of developing ferroelectric film based metasurface devices, which is expected to be applied in terahertz wireless communication in the future.

Funding

This work was supported by the National Natural Science Foundation of China (U23A20279).

Conflicts of interest

The authors have nothing to disclose.

Data availability statement

The data that support the findings of this study are available from the corresponding authors upon reasonable request.

Author contribution statement

Conceptualization, Y. F. and X. F.; Methodology, Y. F., X. F., and Y. G.; Software, Y. F.; Validation, Y. F. and X. F.; Data Curation, X. F.; Investigation, Y. F.; Resources, X. F.; Writing – Original Draft Preparation, Y. F.; Writing – Review & Editing, X. F. and Y. G.; Supervision, X. F. and Y. G.; Project Administration, X. F.; Funding Acquisition, X. F.

References

1. T.J. Cui, M. Q. Qi, X. Wan, J. Zhao, Q. Cheng, Coding metamaterials, digital metamaterials and programmable metamaterials, *Light Sci. Appl.* **3**, e218 (2014)
2. S. Liu, T.J. Cui, Q. Xu, D. Bao, L. Du, X. Wan, W.X. Tang, C. Ouyang, X.Y. Zhou, H. Yuan, H.F. Ma, W.X. Jiang, J. Han, W. Zhang, Q. Cheng, Anisotropic coding metamaterials and their powerful manipulation of differently polarized terahertz waves, *Light Sci. Appl.* **5**, e16076 (2016)
3. L. Bi, J. Hu, P. Jiang, D.H. Kim, G.F. Dionne, L.C. Kimerling, C.A. Ross, On-chip optical isolation in monolithically integrated non-reciprocal optical resonators, *Nat. Photonics* **5**, 758 (2011)
4. V. Kuzmiak, S. Eyderman, M. Vanwolleghem, Controlling surface plasmon polaritons by a static and/or time-dependent external magnetic field, *Phys. Rev. B* **86**, 045403 (2012)
5. X. Zhang, W. Li, X. Jiang, Confined one-way mode at magnetic domain wall for broadband high-efficiency one-way waveguide, splitter and bender, *Appl. Phys. Lett.* **100**, 041108 (2012)
6. H. Lu, B. Zheng, T. Cai, C. Qian, Y. Yang, Z. Wang, H. Chen, Frequency-controlled focusing using achromatic metasurface, *Adv. Opt. Mater.* **9**, 2001311 (2021)
7. B. Xiong, Y. Xu, J. Wang, L. Li, L. Deng, F. Cheng, R. Peng, M. Wang, Y. Liu, Realizing colorful holographic mimicry by metasurfaces, *Adv. Mater.* **33**, 2005864 (2021)
8. N.K. Grady, J.E. Heyes, D.R. Chowdhury, Y. Zeng, M.T. Reiten, A.K. Azad, A.J. Taylor, D.A.R. Dalvit, H.-T. Chen, Terahertz metamaterials for linear polarization conversion and anomalous refraction, *Science* **340**, 1304 (2013)
9. J. Tang, X. Meng, H. Shi, J. Yi, X. Chen, G.-L. Huang, J. Manuel Fernández González, Q. Cheng, Wideband optically transparent low-profile holographic impedance metasurface for multimode OAM generation, *IEEE Trans. Microw. Theory Tech.* **73**, 726 (2025)
10. S. Li, K.L. Tsakmakidis, T. Jiang, Q. Shen, H. Zhang, J. Yan, S. Sun, L. Shen, Unidirectional guided-wave-driven metasurfaces for arbitrary wavefront control, *Nat. Commun.* **15**, 5992 (2024)
11. W. Li, Q. Ma, C. Liu, Y. Zhang, X. Wu, J. Wang, S. Gao, T. Qiu, T. Liu, Q. Xiao, J. Wei, T.T. Gu, Z. Zhou, F. Li, Q. Cheng, L. Li, W. Tang, T.J. Cui, Intelligent metasurface system for automatic tracking of moving targets and wireless communications based on computer vision, *Nat. Commun.* **14**, 989 (2023)

12. J.C. Liang, Q. Cheng, Y. Gao, C. Xiao, S. Gao, L. Zhang, S. Jin, T.J. Cui, An angle-insensitive 3-Bit reconfigurable intelligent surface, *IEEE Trans. Antennas Propag.* **70**, 8798 (2022)
13. H. Zhang, Z. Zhang, X. Ma, C. Huang, M. Pu, J. Luo, X. Zhang, Q. Xiong, Y. Wang, X. Luo, Active matrix integrated metasurface for 2D electromagnetic modulation, *Adv. Opt. Mater.* **12**, 2301631 (2023)
14. H. Jeong, E. Park, R. Phon, S. Lim, Mechatronic reconfigurable intelligent-surface-driven indoor fifth-generation wireless communication, *Adv. Intell. Syst.* **4**, 2200185 (2022)
15. C. Lor, R. Phon, S. Lim, Reconfigurable transmissive metasurface with a combination of scissor and rotation actuators for independently controlling beam scanning and polarization conversion, *Microsyst. Nanoeng.* **10**, 40 (2024)
16. E. Wang, G. Peng, K. Zhong, F. Wu, Z.H. Jiang, R. Sauleau, W. Hong, A 1296-cell reconfigurable reflect-array antenna with 2-bit phase resolution for Ka-band applications, *IEEE Trans. Antennas Propag.* **72**, 3425 (2024)
17. J.C. Liang, Y. Gao, Z.W. Cheng, R.Z. Jiang, J.Y. Dai, L. Zhang, Q. Cheng, S. Jin, T.J. Cui, An optically transparent reconfigurable intelligent surface with low angular sensitivity, *Adv. Opt. Mater.* **12**, 2202081 (2024)
18. X. Li, R. Xu, X. Sun, Y. Zhao, Z. Yang, G. Du, Broadband intelligent programmable metasurface with polarization-modulated self-adaptive electromagnetic functionality switching, *Photon. Res.* **12**, 1395 (2024)
19. J. Wu, Z. Shen, S. Ge, B. Chen, Z. Shen, T. Wang, C. Zhang, W. Hu, K. Fan, W. Padilla, Y. Lu, B. Jin, J. Chen, P. Wu, Liquid crystal programmable metasurface for terahertz beam steering, *Appl. Phys. Lett.* **116**, 131104 (2020)
20. C.X. Liu, F. Yang, X.J. Fu, J.W. Wu, L. Zhang, J. Yang, T.J. Cui, Programmable manipulations of terahertz beams by transmissive digital coding metasurfaces based on liquid crystals, *Adv. Opt. Mater.* **9**, 2100932 (2021)
21. X. Fu, L. Shi, J. Yang, Y. Fu, C. Liu, J.W. Wu, F. Yang, L. Bao, T.J. Cui, Flexible terahertz beam manipulations based on liquid-crystal-integrated programmable metasurfaces, *ACS Appl. Mater. Interfaces* **14**, 22287 (2022)
22. C. Chen, S. Chen, Y. Ni, Y. Xu, Y. Yang, Liquid crystal metasurface for on-demand terahertz beam forming over 110° field-of-view, *Laser Photonics Rev.* **18**, 2400237 (2024)
23. S. Dash, C. Psomas, I. Krikidis, I.F. Akyildiz, A. Pitsillides, Active control of THz waves in wireless environments using graphene-based RIS, *IEEE Trans. Antennas Propag.* **70**, 8785 (2022)
24. G. Guo, X. Zhang, L. Niu, T. Wu, X. Chen, Q. Xu, J. Han, W. Zhang, Programmable graphene metasurface for terahertz propagation control based on electromagnetically induced transparency, *Carbon* **208**, 345 (2023)
25. B. Chen, X. Wang, W. Li, C. Li, Z. Wang, H. Guo, J. Wu, K. Fan, C. Zhang, Y. He, B. Jin, J. Chen, P. Wu, Electrically addressable integrated intelligent terahertz metasurface, *Sci. Adv.* **8**, eadd1296 (2022)
26. H. Guo, B. Chen, Y. Li, W. Li, S. Yang, S. Wang, W. Zhu, J. Wu, H. Ma, X. Zhang, C. Zhang, K. Fan, H. Wang, B. Jin, J. Chen, P. Wu, Broadband, transmissive, and cascable terahertz programmable metasurface, *ACS Nano* **19**, 21660 (2025)
27. B. Dong, S. Zhu, G. Guo, T. Wu, X. Lu, W. Huang, H. Ma, Q. Xu, J. Han, S. Zhang, Y. Wang, X. Zhang, L. Huang, Switchable pancharatnam-berry phases in heterogeneously integrated THz metasurfaces, *Adv. Mater.* **37**, 2417183 (2025)
28. Q. Lin, H. Wong, L. Huitema, A. Crunteanu, Coding metasurfaces with reconfiguration capabilities based on optical activation of phase-change materials for terahertz beam manipulations, *Adv. Opt. Mater.* **10**, 2101699 (2022)
29. S. Prakash, P. Pitchappa, P. Agrawal, H. Jani, Y. Zhao, A. Kumar, J. Thong, J. Linke, A. Ariando, R. Singh, T. Venkatesan, Electromechanically reconfigurable terahertz stereo metasurfaces, *Adv. Mater.* **36**, 2402069 (2024)
30. K.K. Karnati, Y. Shen, M.E. Trampler, S. Ebadi, P.F. Wahid, X. Gong, A BST-integrated capacitively loaded patch for Ka- and X-band beamsteerable reflectarray antennas in satellite communications, *IEEE Trans. Antennas Propag.* **63**, 1324 (2015)
31. L. Wu, T. Du, N. Xu, C. Ding, H. Li, Q. Sheng, M. Liu, J. Yao, Z. Wang, X. Lou, W. Zhang, A new Ba_{0.6}Sr_{0.4}TiO₃-silicon hybrid metamaterial device in terahertz regime, *Small* **12**, 2610 (2016)
32. M. Nikfalazar, M. Sazegar, A. Mehmood, A. Wiens, A. Friederich, H. Maune, J.R. Binder, R. Jakoby, Two-dimensional beam-steering phased-array antenna with compact tunable phase shifter based on BST thick films, *IEEE Antennas Wireless Propag. Lett.* **16**, 585 (2017)
33. D. Shreiber, W. Zhou, G. Dang, M. Taysing-Lara, G. Metcalfe, E. Ngo, M. Ivill, S.G. Hirsch, M. W. Cole, Tunable metamaterial device for THz applications based on BaSrTiO₃ thin film, *Thin Solid Films* **660**, 282 (2018)
34. B. Dong, H. Ma, J. Wang, P. Shi, J. Li, L. Zhu, J. Lou, M. Feng, S. Qu, A thermally tunable THz metamaterial frequency-selective surface based on barium strontium titanate thin film, *J. Phys. D: Appl. Phys.* **52**, 045301 (2019)
35. Q. Tang, Z. Shi, S. Xia, X. Bie, Y. Yang, D. Bian, D. Xu, R. Fan, Enhanced dielectric properties of Sr²⁺ and Zr⁴⁺ doped BaTiO₃ colossal permittivity metamaterials, *EPJ Appl. Metamat.* **11**, 13 (2024)
36. M. Aldrigo, A.C. Tasolamprou, D. Vasilache, M. Kafesaki, S. Iordanescu, F. Nastase, M. Dragoman, Tunable microwave dual-band patch antenna through integration of metamaterials and nanoscale ferroelectrics, *Phys. Rev. Appl.* **20**, 044067 (2023)
37. M. Sazegar, Y. Zheng, C. Kohler, H. Maune, M. Nikfalazar, J.R. Binder, R. Jakoby, Beam steering transmitarray using tunable frequency selective surface with integrated ferroelectric varactors, *IEEE Trans. Antennas Propag.* **60**, 5690 (2012)
38. K.K. Karnati, M.E. Trampler, X. Gong, A monolithically BST-integrated Ka-band beamsteerable reflectarray antenna, *IEEE Trans. Antennas Propag.* **65**, 159 (2017)
39. X. Fu, Y. Guo, J. Zhou, Terahertz optical parameters and lattice vibration-induced resonance of Er³⁺-doped Y₃Al₅O₁₂ crystal, *J. Electromagn. Waves Appl.* **27**, 1792 (2013)

40. I. Kawayama, K. Kotani, M. Misra, H. Murakami, M. Tonouchi, Dielectric properties of (Ba,Sr)TiO₃ thin films in MHz and THz frequency regions: Quantitative evaluation of the orientational polarization, *Jpn. J. Appl. Phys.* **53**, 09PD06 (2014)
41. L. Wu, Y. Fu, N. Xu, Q. Sheng, X. Zhang, Y. Yang, J. Yao, D. Xu, X. Ding, J. Li, Z. Wang, W. Zhang, Observation of Phase Transitions of Ba_{0.6}Sr_{0.4}TiO₃-Silicon Hybrid Metamaterial by THz Spectra, *ACS Appl. Electron. Mater.* **2**, 2449 (2020)

Cite this article as: Yuan Fu, Xiaojian Fu, Yunsheng Guo, Terahertz metasurface enabled by barium strontium titanate ferroelectric film, *EPJ Appl. Metamat.* **13**, 9 (2026), <https://doi.org/10.1051/epjam/2026003>